Exclusive ρ^0 and ϕ muoproduction at large Q^2

New Muon Collaboration

M. Arneodo [m,4], A. Arvidson [n], B. Badełek [n,p], M. Ballintijn [i], G. Baum [a],
J. Beaufays [i,5], I.G. Bird [i,6], P. Björkholm [n], M. Botje [ℓ,7], C. Broggini [h,8],
W. Brückner [d], A. Brüll [c,9], W.J. Burger [ℓ,10], J. Ciborowski [p],
R. van Dantzig [i], A. Dyring [n], H. Engelien [c,11], M.I. Ferrero [m], L. Fluri [h],
U. Gaul [d], T. Granier [j], D. von Harrach [d,12], M. van der Heijden [i,7],
C. Heusch [k], Q. Ingram [ℓ], K. Janson-Prytz [n,13], M. de Jong [i],
E.M. Kabuß [d,12], R. Kaiser [c], T.J. Ketel [i], F. Klein [f], S. Kullander [n],
K. Kurek [p], U. Landgraf [c], T. Lindqvist [n], G.K. Mallot [f], C. Mariotti [m,14],
G. van Middelkoop [b,i], Y. Mizuno [d,15], A. Most [d], A. Mücklich [d],
J. Nassalski [b,o], D. Nowotny [d,16], J. Oberski [i], A. Paić [h], C. Peroni [m],
B. Povh [d,e], R. Rieger [f,17], K. Rith [d,18], K. Röhrich [f,19], E. Rondio [o],
L. Ropelewski [p], A. Sandacz [o], D. Sanders [20], C. Scholz [d,16], R. Seitz [f],
F. Sever [i,21], T.-A. Shibata [e], M. Siebler [a], A. Simon [d], A. Staiano [m],
M. Szleper [o], Y. Tzamouranis [d,20], J.L. Vuilleumier [h], T. Walcher [f],
R. Windmolders [g], A. Witzmann [c], F. Zetsche [d]

[a] *Bielefeld University, Bielefeld, Germany* [1]
[b] *CERN, Geneva, Switzerland*
[c] *Freiburg University, Freiburg, Germany* [1]
[d] *Max-Planck Institut für Kernphysik, Heidelberg, Germany* [1]
[e] *Heidelberg University, Heidelberg, Germany* [1]
[f] *Mainz University, Mainz, Germany* [1]
[g] *Mons University, Mons, Belgium*
[h] *Neuchatel University, Neuchatel, Switzerland*
[i] *NIKHEF-K, Amsterdam, The Netherlands* [2]
[j] *Saclay DAPNIA/SSP, Paris, France*
[k] *University of California, Santa Cruz, USA*
[ℓ] *Paul Scherrer Institute, Villigen, Switzerland*
[m] *Torino University and INFN Torino, Turin, Italy*
[n] *Uppsala University, Uppsala, Sweden*
[o] *Soltan Institute for Nuclear Studies, Warsaw, Poland* [3]
[p] *Warsaw University, Warsaw, Poland* [3]

Abstract

Exclusive ρ^0 and ϕ muoproduction on deuterium, carbon and calcium has been studied in the kinematic range $2 < Q^2 < 25\,\text{GeV}^2$ and $40 < \nu < 180\,\text{GeV}$. We discuss the Q^2 dependence of the cross sections, the transverse momentum distributions for the vector mesons, the decay angular distributions and, in the case of the ρ^0, nuclear effects. The data for ρ^0 production are compatible with a diffractive mechanism. The distinct features of ϕ production are a smaller cross section and less steep p_t^2 distributions than those for the ρ^0 mesons.

1. Introduction

In this paper we present results on exclusive ρ^0 and ϕ production in Deep Inelastic Scattering (DIS) of muons on deuterium, carbon and calcium. The experiment was carried out at CERN by the New Muon Collaboration (NMC) using a 200 GeV muon beam. The data discussed here were partially covered in Ref. [1]. The present paper extends and supersedes the results presented there.

The exclusive ρ^0 (or ϕ) production reaction is

$$\mu + N \rightarrow \mu + N + \rho^0 \ (\text{or}\ \phi), \tag{1}$$

in which the only particle produced is the ρ^0 (or ϕ) meson. This is sometimes referred to as elastic production. If the target is a nucleus which remains intact, the reaction is coherent. In incoherent reactions nucleons are ejected from the nucleus by the interaction.

[1] Supported by Bundesministerium für Forschung und Technologie.

[2] Supported in part by FOM, Vrije Universiteit Amsterdam and NWO.

[3] Supported by KBN SPUB Nr 621/E - 78/SPUB/P3/209/94.

[4] Now at Dipartimento di Fisica, Università della Calabria, I-87036 Arcavacata di Rende (Cosenza), Italy.

[5] Now at Trasys, Brussels, Belgium.

[6] Now at CERN, 1211 Geneva 23, Switzerland.

[7] Now at NIKHEF-H 1009 DB Amsterdam, The Netherlands.

[8] Now at University of Padova, 35131 Padova, Italy.

[9] Now at MPI für Kernphysik, 69029 Heidelberg, Germany.

[10] Now at Université de Genève, 1211 Geneva 4, Switzerland.

[11] Now at LHS GmbH, 63303 Dreieich, Germany.

[12] Now at University of Mainz, 55099 Mainz, Germany.

[13] Now at DESY, Notkestraße 85, 2000 Hamburg, Germany.

[14] Now at INFN-Istituto Superiore di Sanità, 00161 Rome, Italy.

[15] Now at Osaka University, 567 Osaka, Japan.

[16] Now at SAP AG, 6909 Walldorf, Germany.

[17] Now at Ploenzke Informatik, 6800 Mannheim, Germany.

[18] Now at University of Erlangen-Nürnburg, 91058 Erlangen, Germany.

[19] Now at IKP2-KFA, 5170 Jülich, Germany.

[20] Now at University of Houston, 77204 Texas, U.S.A.

Funded by NSF and DOE.
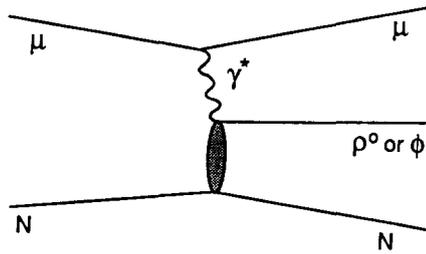
[21] Now at ESRF, 38043 Grenoble, France.

Fig. 1. Diagram of the exclusive muoproduction of vector mesons.

The reactions can be viewed as proceeding according to the diagram shown in Fig. 1 and thus can be described in terms of the virtual photoproduction process $\gamma^* N \to \rho^0(\phi) N$.

The quantum numbers of the ρ^0 and ϕ mesons, $J^{PC} = 1^{--}$, are the same as those of the photon. Hence one can describe the above photoproduction process by the exchange of a colourless object carrying the vacuum quantum numbers, commonly referred to as the pomeron. The pomeron was traditionally used to describe diffractive hadronic interactions [2]. In real photoproduction and small Q^2 electroproduction of vector mesons the characteristic features of diffractive processes are also observed [3]. The similarity to hadronic processes has been accounted for in the framework of the Vector Meson Dominance (VMD) model, in which it is assumed that photons fluctuate into vector mesons of the same quantum numbers.

At large Q^2, it may be more useful to describe the photon as fluctuating into quark–antiquark pairs than into hadrons. Further, the γ^*–N interaction may be described in perturbative QCD in terms of the exchange of two gluons between the nucleon and the virtual q-$\bar{q}$ pair. In addition the q-$\bar{q}$ pair transverse separation, and hence interaction probability, decreases with increasing Q^2. Both hadronic (VMD) and PQCD descriptions may be appropriate in the kinematic range of this experiment.

The paper is organised as follows. After a brief review of the experimental and theoretical status of the field, we describe our ρ^0 sample. We present cross sections as a function of Q^2 and ν of the virtual photon and as a function of the transverse momentum of the mesons with respect to the virtual photon direction. The nuclear dependence of the cross sections is presented. The angular distributions of the decay particles and R, the ratio of the longitudinal to transverse virtual photoproduction cross sections, are also discussed. The exclusive ϕ production results are then similarly presented.

Kinematic variables used in this paper are listed in Table 1.

1.1. Results of previous experiments and theoretical models

Exclusive virtual photoproduction of ρ^0 and ϕ mesons has been extensively investigated [3–6] at small Q^2 (< 2 GeV^2) while at larger Q^2 only few experimental results are available [6–8].

We briefly summarise the main characteristics of the small Q^2 data.
– The shape of the Q^2 dependence of the cross section is well described by VMD: the cross section for production by transversely polarised virtual photons, σ_T, falls with

Table 1
Kinematic variables.

k	Four-momentum of the incident muon
k'	Four-momentum of the scattered muon
p	Four-momentum of the target nucleon
v	Four-momentum of the vector meson V (ρ^0 or ϕ)
$q = k - k'$	Four-momentum of the virtual photon
$-Q^2 = q^2$	Invariant mass squared of the virtual photon
$\nu = (p \cdot q)/M_p$	Energy of the virtual photon in the laboratory system, M_p is the proton mass
$x = Q^2/(2M_p\nu)$	Bjorken scaling variable
$y = (p \cdot q)/(p \cdot k)$	Fraction of the lepton energy lost in the laboratory system
$W^2 = (p + q)^2$	Total energy squared in the $\gamma^* - N$ system
p_t^2	Transverse momentum squared of the vector meson with respect to the virtual photon direction
$m_V = (v^2)^{\frac{1}{2}}$	Invariant mass of the vector meson V
$M_X^2 = (p + q - v)^2$	Missing mass squared of the undetected recoiling system
$I = (M_X^2 - M_p^2)/W^2$	Inelasticity

increasing Q^2 as $(1 + Q^2/m_V^2)^{-2}$, whereas that due to longitudinal photons, σ_L, is proportional to $Q^2(1 + Q^2/m_V^2)^{-2}$.

- The dependence of the cross section on the photon energy, ν, above the resonance region ($\nu > 2$ GeV) is weak.
- The distribution over t, the square of the four-momentum transfer between the virtual photon and the vector meson ($t = (q - v)^2$), is approximately exponential at small $|t|$ values (< 1 GeV^2). For the ρ^0 case, at low energies, the slope of the distribution is about 6–7 GeV^{-2}, rising to about 10 GeV^{-2} at HERA energies. The t-distribution for ϕ production is flatter, with slopes slightly smaller than 4 GeV^{-2}.
- The fraction of longitudinally polarised ρ^0 mesons grows approximately linearly with Q^2 from 0 for real photoproduction ($Q^2 = 0$) to about 0.5 at $Q^2 = 2$ GeV^2.
- s-channel helicity conservation (SCHC), in which the vector meson retains the helicity of the photon, is observed to be approximately valid.
- The nuclear dependence of the cross section is well described by the Glauber multiple scattering model [9] in conjunction with VMD.

At large values of Q^2, the EMC results [7,8] show a different behaviour, with a faster decrease of the cross section with Q^2 and a harder t-dependence than observed for the small Q^2 data. The data also indicate substantial violation of SCHC. Our results on the t-dependence and SCHC do not confirm these features; an explanation for the discrepancy between the t-dependences was already presented in Ref. [1].

The nuclear dependence of coherent and incoherent ρ^0 and ϕ production has recently been investigated by the Fermilab experiment E665 [6]. It was found in particular that the ratio of bound to free nucleon cross sections for exclusive incoherent vector meson production is less than unity.

Several models attempt to describe diffractive vector meson production in DIS [10–16]. All assume pomeron exchange, with the pomeron generally treated as a pair of gluons. Individual models differ however in the way these gluons are described, ranging from non-perturbative approaches [11–13] to perturbative ones [14–16]. Models also

differ in the description of the intermediate quark–antiquark pair and of the vector meson wave function. In spite of these differences, in the kinematic region $Q^2 \gg m_V^2$ and $W^2 \gg Q^2 \gg -t$, all models give qualitatively similar predictions for the cross sections:

- Q^2 dependence of the type $1/Q^6$,
- weak dependence on the virtual photon energy,
- linear growth of $R = \sigma_L/\sigma_T$ as a function of Q^2,
- approximate SCHC.

In this paper R, σ_L and σ_T refer to the exclusive vector meson production process (see Sect. 3.2).

2. Experiment and analysis

The experiment (NMC – NA37) was performed at the M2 muon beam at the CERN SPS. The data presented here were taken during 1987 simultaneously with the structure function measurements [17]. The nominal incident muon energy was 200 GeV. About equal amounts of the data were collected with beams of positive and negative muons.

A complementary target arrangement was used, which was primarily designed to optimise measurements of the ratios of deep inelastic inclusive cross sections from different nuclei. Each target set contained several segments of different material (D, C, Ca) simultaneously exposed to the beam, one behind the other along the beam direction [17]. Events from different targets were well resolved.

The forward spectrometer [18] was used to detect scattered muons and forward hadrons. The apparatus had good efficiency for the detection of charged hadrons of momenta greater than 4 GeV. The data on exclusive ρ^0 and ϕ production were taken with the standard trigger which accepted muons at scattering angles larger than 12 mrad.

The data were processed on an event by event basis [18]. For this analysis we selected events with only two tracks of hadrons of opposite charge associated with the vertex defined by the incident and scattered muon tracks.

The spectrometer allowed identification of muons and electrons. For the present analysis it was essential to remove background from electron pairs from bremsstrahlung photons. For the analysis of the ϕ meson data the electron rejection was done using the information from a calorimeter [19]. The efficiency of the calorimeter to reject a single electron was above 80%. For the analysis of the ρ^0 data the information from the calorimeter was not used. Instead a cut was applied on the invariant mass squared $m^2_{e^+e^-}$ calculated assuming the tracks are due to electrons. The electron rejection methods are discussed in more detail in Sects. 3.1 and 4.1.

A Monte Carlo simulation was used to correct the data for acceptance losses, kinematic smearing and reconstruction efficiencies. The events generated contained exclusive ρ^0 and ϕ mesons produced coherently and incoherently. All outgoing particles, including the scattered muons and radiative photons, were tracked through the target and the apparatus. Secondary interactions of hadrons inside the target, photon conversions and multiple Coulomb scattering were taken into account.

Table 2
Kinematic cuts applied to the data.

Q^2_{min} [GeV^2]	2
ν-range [GeV]	40–190
y_{max}	0.9
Minimum energy of scattered muon [GeV]	20
Minimum hadron momentum [GeV]	4

For each generated event, the responses of the detectors were simulated. These events were then processed in the same way as real events. The overall acceptance for a distribution in a given variable was calculated as the ratio of the distribution obtained after the event processing to the distribution for generated events.

There was no attempt to generate a background to the exclusive processes in the Monte Carlo simulation because, as discussed in Ref. [13], different fragmentation models give substantially different results. The amount of background was estimated from the data, and for each distribution was either subtracted or its effect included in the systematic errors.

In this experiment there was no hadron identification, and so the hadron energies and the value of m_V were calculated both using the pion mass and the kaon mass corresponding to each of two hypotheses: $\rho^0 \to \pi^+ \pi^-$ or $\phi \to K^+ K^-$.

3. Exclusive ρ^0 production

3.1. The event sample

The selection of the ρ^0 meson sample and the corrections applied to the data in the present analysis are similar to those used in Ref. [1]. The few improvements, in the method of electron suppression and in the acceptance calculation, do not significantly change the results reported previously.

To avoid large acceptance corrections and large radiative corrections the kinematic cuts listed in Table 2 were applied to the data. To separate events originating in different target materials, cuts on the coordinates of the interaction vertex were used. The main source of electron background is due to e^+e^- pairs from the conversion of photons. This background was suppressed by a cut

$$m^2_{e^+e^-} > 0.02 \, \text{GeV}^2, \tag{2}$$

where $m^2_{e^+e^-}$ is the invariant mass for a pair of tracks calculated assuming the electron mass for both particles. The loss of exclusive ρ^0 mesons with this cut is negligible. The efficiency for removing electrons from the sample with this cut was checked using the calorimeter data and proved to be high ($\approx 99\%$), resulting in a negligible background.

The exclusive ρ^0 signal is shown in Figs. 2 and 3 for the combined data for the three target nuclei. The distributions for the different nuclei are similar.

In Fig. 2 the acceptance corrected distribution of the two-pion invariant mass, $m_{\pi\pi}$, is given for the events satisfying the Table 2, vertex and $m^2_{e^+e^-}$ cuts mentioned above
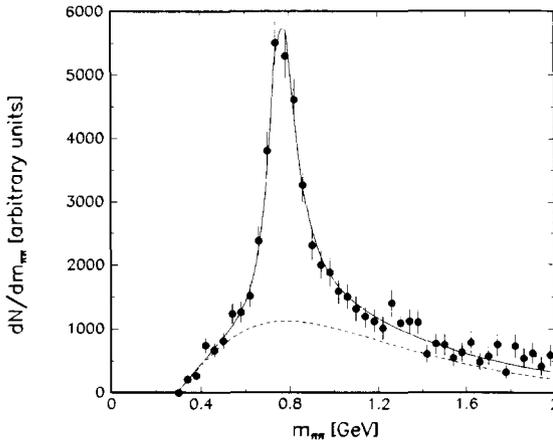
Fig. 2. Acceptance corrected distribution of the two-pion invariant mass. The data from deuterium, carbon and calcium targets were combined. The full line represents the result of a fit assuming the superposition of a p-wave Breit–Wigner and a non-resonant contribution. The broken line shows the non resonant contribution parametrised as $a_0(m_{\pi\pi} - 2m_\pi)^{a_1} e^{-a_2 m_{\pi\pi}}$, where a_0, a_1, a_2 are fitted parameters and m_π is the pion mass.

and an inelasticity cut

$$-0.1 < I < 0.08. \tag{3}$$

From the distribution we excluded those events which, for the hypothesis that the tracks are due to kaons, gave the invariant mass $m_{K^+K^-}$ in the range of the ϕ mass ($1.01 < m_{K^+K^-} < 1.03$ GeV). It was checked with a Monte Carlo calculation that the overlap between the exclusive ρ^0 and ϕ events is negligible ($< 0.2\%$). A superposition of a p-wave Breit–Wigner distribution for the ρ^0 [20] and a non-resonant contribution was fitted to the data. Satisfactory fits were obtained which yielded the ρ^0 mass and width consistent with the known values [21]. No skewing factor was necessary to describe the resonance shape, as also reported previously for large Q^2 data [7], in contrast to the small Q^2 and small $|t|$ data [3]. The full line shows the result of the fit and the broken line the non-resonant contribution. For the central part of the ρ^0 peak, 0.62 GeV $< m_{\pi\pi} < 0.92$ GeV, the non-resonant background contribution is about 25%.

In Fig. 3 the inelasticity distribution uncorrected for acceptance is shown for the data sample satisfying the cuts listed in Table 2, the vertex cuts, the cut on $m^2_{e^+e^-}$ and a cut on the invariant mass

$$0.62 < m_{\pi\pi} < 0.92\,\text{GeV}. \tag{4}$$

The peak at $I = 0$ is the signal of exclusive ρ^0 production. Non-exclusive events, where in addition to detected fast hadrons, slow ($p_h < 4$ GeV) undetected hadrons were produced, appear at $I > 0$. Due to the finite resolution, however, they are not resolved from the exclusive ρ^0 peak. The line shows a parametrisation of the inelasticity distribution for non-exclusive events. It was obtained by fitting the distribution in the near inelastic region ($0.08 < I < 0.20$) with the convolution of a linear dependence and a
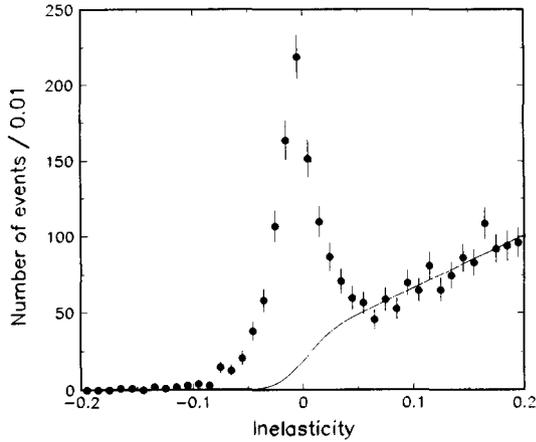
Fig. 3. Inelasticity distribution of ρ^0 mesons uncorrected for acceptance. The data from the deuterium, carbon and calcium targets were combined. The solid line represents the parametrisation of the non-exclusive background described in the text.

Table 3
Numbers of events in the samples of exclusively produced ρ^0 and ϕ mesons.

	Target material			
	D	C	Ca	All
ρ^0	591	266	427	1284
ϕ	44	14	39	97

gaussian describing the known experimental resolution; these fits were then extrapolated to the elastic region. As discussed in Ref. [1] we observe no significant nuclear or Q^2 dependence of the amount of background in the elastic region.

For the region defined by cut (3) the amount of background is 0.23 ± 0.11. On the other hand, in the more restricted range

$$-0.05 < I < 0.00 \tag{5}$$

the amount of background is only 0.04 ± 0.04. For the present analysis we selected two different samples by applying the two inelasticity cuts.

The basic ρ^0 sample was defined using the kinematic cuts listed in Table 2, the vertex cuts and cuts (2)–(4). The number of events for this sample is given in Table 3. This sample is about three times as large as in previous experiments in a similar kinematic range.

For some parts of the analysis (transverse momentum distributions, incoherent cross sections) as well as for cross checks, inelasticity cut (3) was replaced by the more restrictive cut (5). The importance of this for the transverse momentum analysis was discussed in Ref. [1]. Changing the inelasticity cut reduces the number of events by more than a factor of two.

The average values of Q^2 and ν for the two samples are similar, $\langle Q^2 \rangle = 6.3$ GeV^2 and $\langle \nu \rangle = 112$ GeV.

3.2. Virtual photoproduction cross section

We now discuss the cross sections for the process $\gamma^* N \to \rho^0 N$ for different nuclei as a function of Q^2 and ν. They include coherent and incoherent contributions. A discussion of the coherent and incoherent parts separately is given in Sect. 3.4. To facilitate the comparison between different nuclei, the cross sections presented in this paper are always per nucleon.

The total cross section for exclusive ρ^0 production for virtual photons in a given (Q^2, ν) interval may be obtained by normalising the number of events N_ρ corresponding to the reaction

$$\mu N \to \mu \rho^0 N \tag{6}$$

to the total number of scattered muons N_μ for the same interval. Using the cross section of the reaction

$$\mu N \to \mu X, \tag{7}$$

derived from the values of the structure functions of Refs. [17,22], the cross section of reaction (6) is then obtained by the relation

$$\frac{d^2\sigma(\mu N \to \mu\rho^0 N)}{dQ^2 d\nu} \bigg/ \frac{d^2\sigma(\mu N \to \mu X)}{dQ^2 d\nu} = \left(\frac{N_\rho}{\mathcal{A}(\rho|\mu)}\right) \bigg/ (N_\mu \, \eta). \tag{8}$$

Here $\mathcal{A}(\rho|\mu)$ is the conditional probability to observe the ρ^0 when the scattered muon is observed in reaction (6), and η is the radiative correction factor [23] for reaction (7). In the determination of N_ρ, no correction was applied to account for radiative processes. The factor $\mathcal{A}$ accounts for detector acceptance effects estimated by Monte Carlo simulation, losses due to secondary interactions in the target of pions from ρ decay and background corrections. In the latter it was assumed that the non-exclusive and the non-resonant backgrounds are uncorrelated. This assumption is supported by results of fits of the mass distributions obtained with different inelasticity cuts ((3) vs. (5)).

The cross sections for exclusive ρ^0 production and inclusive virtual photon absorption are related to the muon cross sections by

$$\sigma_{\gamma^* N \to \rho^0 N}(Q^2, \nu) = \frac{1}{\Gamma_T} \frac{d^2\sigma(\mu N \to \mu\rho^0 N)}{dQ^2 d\nu}, \tag{9}$$

$$\sigma_{\gamma^* N \to X}(Q^2, \nu) = \frac{1}{\Gamma_T} \frac{d^2\sigma(\mu N \to \mu X)}{dQ^2 d\nu}. \tag{10}$$

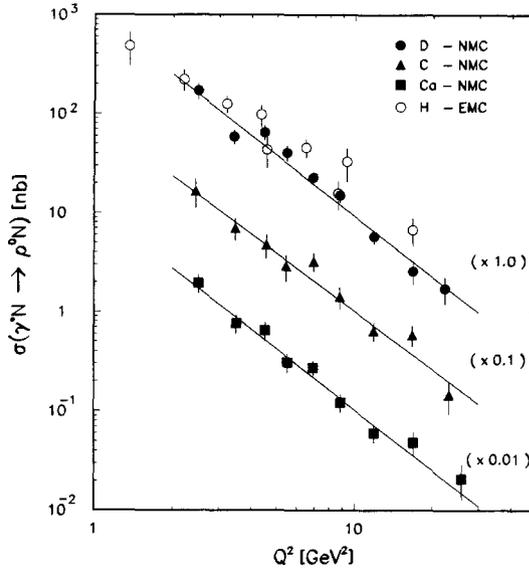Here, Γ_T is the flux of transverse virtual photons

Fig. 4. Exclusive ρ^0 virtual photo-production cross section as a function of Q^2. The data are from the present experiment (full symbols) and from the EMC [7] for the proton (open symbols). The cross sections for carbon and calcium are scaled by factors of 0.1 and 0.01 respectively. The lines are the results of empirical fits to the data described in the text.

$$\Gamma_T = \frac{\alpha(\nu - Q^2/2M_p)}{2\pi Q^2 E_\mu^2 (1 - \epsilon)}, \tag{11}$$

α is the fine structure constant and ϵ is the virtual photon polarisation given by

$$\epsilon = \frac{1 - (\nu/E_\mu) - (Q^2/4E_\mu^2)}{1 - (\nu/E_\mu) + \frac{1}{2}(\nu/E_\mu)^2 + (Q^2/4E_\mu^2)}. \tag{12}$$

The cross section (9) is the sum of two terms due to transverse and longitudinal virtual photons

$$\sigma_{\gamma^* N \to \rho^0 N} = \sigma_T + \epsilon\sigma_L, \tag{13}$$

or equivalently,

$$\sigma_{\gamma^* N \to \rho^0 N} = \sigma_T(1 + \epsilon R), \tag{14}$$

where $R = \sigma_L/\sigma_T$ for the exclusive reaction.

To investigate their Q^2 dependence the cross sections were averaged over ν in each Q^2 bin. We observe no significant dependence on ν as is discussed below.

In Fig. 4 the Q^2 dependence of the cross section for exclusive ρ^0 virtual photoproduction is shown. Also shown are the EMC data on protons [7]. The cross sections measured in this experiment are also given in Table 4 together with the mean values $\langle\nu\rangle$ and $\langle\epsilon\rangle$ for each Q^2 bin. The errors shown are statistical; the systematic errors are

Table 4

Total cross sections $\sigma(\gamma^*N \to \rho^0 N)$ as a function of Q^2. For each Q^2 bin the average ν and ϵ are indicated. The errors are statistical. There is an additional normalisation uncertainty of about 20%.

Q^2 [GeV^2]	$\langle \nu \rangle$ [GeV]	$\langle \epsilon \rangle$	$\sigma(\gamma^*N \to \rho^0 N)$ [nb]
		Deuterium	
2.5	140	0.50	170 ± 31
3.5	116	0.66	60 ± 10
4.5	117	0.66	65 ± 11
5.5	106	0.72	41 ± 7
6.9	99	0.76	23 ± 3
8.8	93	0.78	15 ± 2
11.9	87	0.82	5.8 ± 0.9
16.9	87	0.81	2.6 ± 0.7
22.5	92	0.80	1.7 ± 0.5
		Carbon	
2.4	146	0.45	165 ± 54
3.5	139	0.52	70 ± 18
4.6	122	0.62	47 ± 13
5.5	116	0.67	29 ± 9
7.0	97	0.77	32 ± 7
8.8	94	0.77	14 ± 4
11.9	87	0.82	6.4 ± 1.3
16.8	92	0.79	5.9 ± 1.4
23.1	85	0.86	1.5 ± 0.5
		Calcium	
2.5	139	0.52	192 ± 41
3.5	124	0.61	76 ± 17
4.5	104	0.72	64 ± 14
5.5	101	0.74	31 ± 7
6.9	94	0.78	27 ± 5
8.9	90	0.80	12 ± 3
11.9	87	0.82	6.0 ± 1.2
16.9	100	0.76	4.8 ± 1.3
25.9	96	0.79	2.1 ± 0.8

about 20% (25% for the data of Ref. [7]). The dominant contribution to the systematic error comes from uncertainties in the background estimates and is common to all data points. This error is thus largely independent of Q^2, ν and A.

The measured total cross sections for carbon and calcium are close to those for deuterium. Fig. 4 indicates fair agreement between the proton [7] and deuteron data. It should be noted that the cross sections depend both on R, which may be Q^2 dependent, and ϵ which was lower in this experiment (see Table 4) than in Ref. [7], where $\langle \epsilon \rangle$ was 0.84. At $Q^2 = 6$ GeV^2, using $R = 2.0$ as obtained in Sect. 3.5, this accounts for about a quarter of the difference.
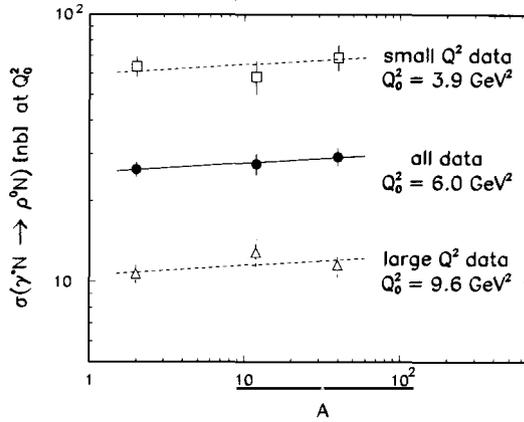
Fig. 5. The exclusive ρ^0 virtual photoproduction cross section as a function of atomic mass, A, evaluated at $Q^2 = Q_0^2$. The full points were obtained using all data; the open symbols are for the data at small and large Q^2. The full line shows a parametrisation $\propto A^\delta$, fitted to all data. The dashed lines have the same slope and were scaled to the data at the other Q_0^2 values.

Table 5

Total cross sections (coherent + incoherent) per nucleon for the $\gamma^* N \longrightarrow \rho^0 N$ reaction at $Q^2 = Q_0^2$. The errors are statistical. There is an additional normalisation uncertainty of about 20%.

Q^2 range [GeV^2]	Q_0^2 [GeV^2]	D	C	Ca
2–25	6.0	26.2 ± 1.6 nb	27.4 ± 2.5 nb	29.2 ± 2.2 nb
2–6	3.9	64.1 ± 5.8 nb	58.6 ± 8.3 nb	69.1 ± 7.6 nb
6–25	9.6	10.7 ± 0.9 nb	12.9 ± 1.5 nb	11.6 ± 1.2 nb

To compare the Q^2 dependence for the different nuclei, we have parametrised the data according to

$$\sigma(Q^2) = \sigma_0 \left(\frac{Q_0^2}{Q^2} \right)^\beta , \tag{15}$$

where σ_0 and β are fitted parameters and Q_0^2 is set equal to the average Q^2 of a given data sample. The fits yield values for β of 2.05±0.09 for deuterium, 1.96±0.13 for carbon and 2.04±0.13 for calcium. These fits are shown in Fig. 4. The results of the fits are compatible and a combined fit to all data yields $\beta = 2.02 \pm 0.07$.

The values of σ_0, the cross section at $Q^2 = Q_0^2$, determined for various Q_0^2 and ranges of Q^2, are given in Table 5 and Fig. 5. The dependence of the cross section on the atomic number A can be parametrised as $\propto A^\delta$, with $\delta = 0.035 \pm 0.032$. The result is compatible with no A dependence.

The ν dependence of the cross section σ_0 is given in Fig. 6 at $Q^2 = 6$ GeV^2. There is no significant variation between $\nu = 70$ and 140 GeV. Fig. 6 also shows the transverse cross section derived using Eq. (14), taking $R = 2.0 \pm 0.3$ (Sect. 3.5). It was assumed that R does not vary with ν.
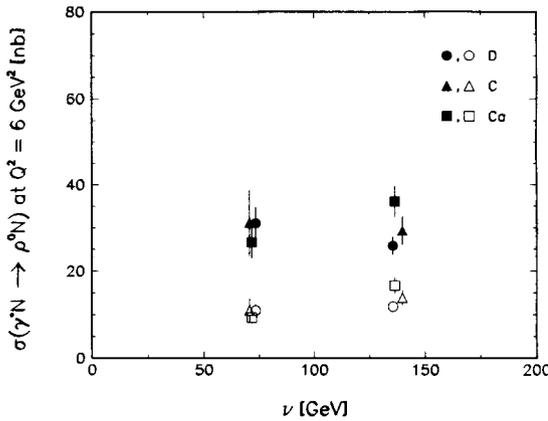
Fig. 6. The ν dependence of the exclusive ρ^0 virtual photoproduction cross sections for different targets at $Q^2 = 6$ GeV^2. Full symbols correspond to the measured total cross sections, the open symbols to the cross sections for the transversely polarised photons.

In order to search further for possible nuclear effects we studied the ratio of the average cross sections for carbon and calcium to that for deuterium. In Fig. 7 this ratio is shown as a function of Q^2, $l_c = 2\nu/(Q^2 + m_\rho^2)$ and $x = Q^2/(2M_p\nu)$. The variable l_c can be viewed as the length of the virtual ρ^0 fluctuation of the virtual photon in the laboratory system [3]. The ratios are everywhere consistent with unity.

In conclusion, we observe that the cross sections are approximately proportional to $1/Q^4$ in the range $2 < Q^2 < 25$ GeV^2. The data show no significant ν dependence. The cross sections do not appear to depend on the atomic number A.

3.3. The transverse momentum distributions

In this section we present the differential cross sections $d\sigma/dp_t^2$ and give parametrisations of them to facilitate comparisons with other experiments and with models. The results on transverse momentum distributions were partly covered in previous publications [1,24]. The effect of the non-exclusive background on the transverse momentum distributions and the ways to reduce it were discussed in Ref. [1].

In Fig. 8 the differential cross sections for the different nuclei are shown. They were obtained from the data in the range $2 < Q^2 < 25$ GeV^2 and were normalised to the virtual photoproduction total cross sections at $Q^2 = 6$ GeV^2. The p_t^2 distributions given here were obtained with the restrictive inelasticity cut (5)*. We observe clear coherent peaks at small p_t^2 values (< 0.05 GeV^2) and less steep distributions for the incoherent events.

We present the p_t^2-slopes for the incoherent events in Table 6. The function

$$\frac{d\sigma}{dp_t^2} = a\, e^{-b_{in}p_t^2} \tag{16}$$

---

* The distributions shown in Fig. 3 of Ref. [1] were given for a different inelasticity cut.
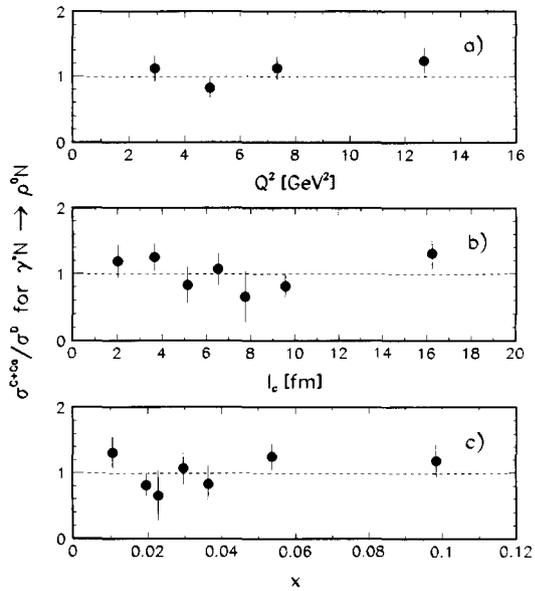
Fig. 7. The ratio of exclusive ρ^0 virtual photoproduction cross section for C and Ca combined with respect to that for deuterium, as a function of different kinematic variables.
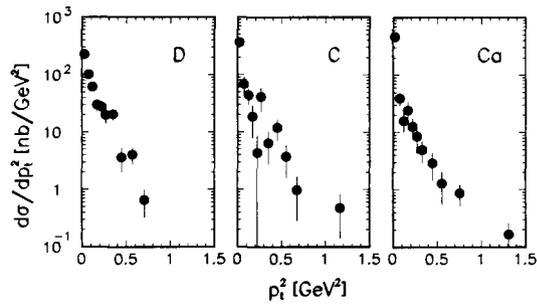

Fig. 8. The p_t^2 distributions for different nuclei. The cross sections were obtained with the restrictive inelasticity cut (5) to reduce the effect of the non-exclusive background.

Table 6
The fitted p_t^2-slopes in $[\text{GeV}^{-2}]$ for incoherent events. The fits were made in the range $0.2 < p_t^2 < 1.0\,\text{GeV}^2$ for the interval $2 < Q^2 < 25\,\text{GeV}^2$. The errors are statistical. There is an additional systematic error of 0.7 GeV^{-2}.

D	7.1 ± 0.9
C	4.5 ± 1.5
Ca	5.4 ± 1.2
All	6.3 ± 0.6

was fitted to the p_t^2 distributions in the range $0.2 < p_t^2 < 1.0$ GeV^2. The lower cut was introduced to eliminate coherent events. The fitted slopes are given for the different nuclear targets separately and for the combined data. The quoted errors are statistical; the systematic error is 0.7 GeV^{-2} [1].

The average p_t^2-slope for incoherent events for the combined data in the full Q^2 interval is $b_{in} = 6.3 \pm 0.6 \pm 0.7$ GeV^{-2}. In the more restricted Q^2 interval 6–25 GeV^2, b_{in} is 4.6 ± 0.8 GeV^{-2}, consistent with our earlier work (4.3 ± 0.6 GeV^{-2}) [1]. The slope for the full Q^2 range corresponds to a mean p_t^2 value of $\langle p_t^2 \rangle = 0.16\pm0.015\pm0.018$ GeV^2 for the exclusive production of ρ^0 mesons on a single nucleon. This value is substantially smaller than the mean p_t^2 values (0.6–0.7 GeV^2) for leading hadrons ($z > 0.5$, where z is the fraction of the photon energy carried by the hadron) produced in inclusive deep inelastic scattering in comparable Q^2 and W^2 ranges [25]. This indicates that the mechanism of exclusive ρ^0 production is different from that for hadron production in inclusive hard scattering processes.

We do not present the p_t^2-slopes of the coherent peaks because due to kinematic smearing they are poorly determined. However, the coherent cross sections integrated over p_t^2 are much less sensitive to smearing. We parametrised the full p_t^2 distributions in the following way:

$$\frac{d\sigma}{dp_t^2} = \sigma_{tot} \left\{ c \, b_{coh} \, e^{-b_{coh}p_t^2} + (1-c) \, b_{in} \, e^{-b_{in}p_t^2} \right\}. \tag{17}$$

The values of the slopes for incoherent events, b_{in}, were fixed to be those of Table 6. The slopes for coherent events were taken to be $b_{coh} = \langle r^2 \rangle/3$, where $\langle r^2 \rangle$ is the mean square radius of the charge distribution of a nucleus. The values of b_{coh} used for deuterium, carbon and calcium were 38.0, 52.2 and 103.7 GeV^{-2}, respectively. The total cross section σ_{tot} is that given in Table 5 for the full Q^2 range. The parameter c, which quantifies the p_t^2-integrated relative contributions of the two exponentials, was found from the fit. The values determined for c do not depend significantly on those assumed for b_{coh}.

The values of c determined for the deuterium, carbon and calcium targets are 0.23 ± 0.10, 0.70 ± 0.09 and 0.71 ± 0.06, respectively. No significant Q^2 dependence of c was found. Our results do not agree with those of Ref. [8], which however were affected by non-exclusive background [1].

3.4. Nuclear dependence of the incoherent and coherent cross sections

In Sect. 3.2 we have shown that there is no A dependence of the total cross sections. In this section we investigate the nuclear dependence of the incoherent cross sections presented in terms of the nuclear transparency for carbon and calcium, as well as the ratios of the integrated coherent cross sections for these nuclei. The data are compared with the results of the experiment E665 [6].

Nuclear transparency is defined by

$$T = \frac{d\sigma_{in}^{nucleus}}{dp_t^2} \bigg/ \frac{d\sigma_{in}^{D}}{dp_t^2}, \tag{18}$$

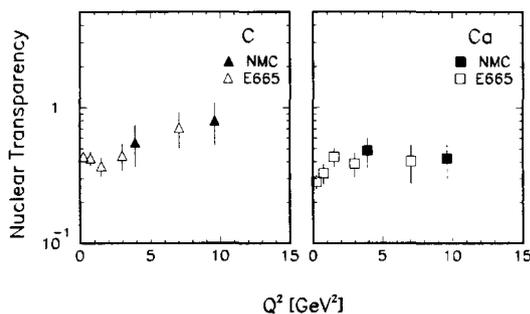*New Muon Collaboration/Nuclear Physics B 429 (1994) 503–529*

Fig. 9. The Q^2 dependence of the nuclear transparency T for incoherent exclusive ρ^0 virtual photoproduction. The data are from the present experiment (full symbols) and the preliminary data from E665 [6] (open symbols).
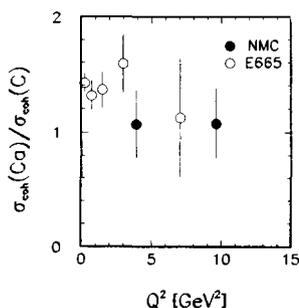

Fig. 10. The Q^2 dependence of the ratio $\sigma_{coh}^{Ca}/\sigma_{coh}^{C}$ for coherent ρ^0 virtual photoproduction. The data are from the present experiment (full symbols) and the preliminary data from E665 [6] (open symbols).

where σ_{in} is the incoherent cross section evaluated in the range where coherent effects are negligible. The nuclear transparencies were obtained by fitting formula (16) to the data in the range $0.1 < p_t^2 < 1.0$ GeV^2 with a common slope b_{in} for all nuclei, and dividing the normalisation coefficients, a, for carbon or calcium by that for deuterium. The resulting transparencies are $T = 0.51 \pm 0.13$ and 0.44 ± 0.08 for carbon and calcium, respectively, with an estimated systematic error of 0.10. The nuclear transparencies obtained for two Q^2 ranges are shown in Fig. 9, in which the preliminary results of the experiment E665 [6] are also displayed. The present results confirm the nuclear mass dependence of the incoherent cross section seen in experiment E665.

The total exclusive cross sections (Table 5) together with the values of the parameter c describing the p_t^2 distributions (see previous section) were used to calculate the p_t^2-integrated coherent cross sections. They were corrected for the effects of the finite minimum four-momentum transfer t_{min} and for the suppression of incoherent cross sections at small p_t^2 [9]. The correction for finite minimum four-momentum transfer is equal to 1.02–1.04 for carbon and 1.17–1.40 for calcium depending on Q^2 and ν. The correction for suppression of the incoherent events at small p_t^2 is equal 1.09 for carbon and 1.03 for calcium. In Fig. 10 we show the ratio $\sigma_{coh}^{Ca}/\sigma_{coh}^{C}$ for the present data for

two Q^2 ranges together with the preliminary results of the E665 experiment.

3.5. Rho decay angular distributions

In this section, from the analysis of the ρ^0 decay polar angle distributions, we determine the fractions of ρ^0 mesons produced with longitudinal polarisation (helicity 0). Further, we present azimuthal angular distributions which indicate the consistency of the data with the hypothesis of s-channel helicity conservation (SCHC). Assuming SCHC and using the measured fractions of longitudinally polarised ρ^0 mesons, we determine the ratio R of cross sections for exclusive ρ^0 production by longitudinal and transverse virtual photons.

The ρ decay acts as an analyzer of its spin states. Hence the analysis of the decay distributions allows us to study spin-dependent properties of the production process. The relevant formalism has been developed in Ref. [26].

Usually the ρ^0 decay angular distribution $W(\cos\theta, \phi, \Phi)$ is studied in the s-channel helicity frame, which is the most convenient for describing the ρ decay after photo- and electroproduction [3,27,28]. The ρ^0 direction in the virtual photon-nucleon centre of mass system is taken as the quantisation axis. The angle θ is the polar angle and ϕ the azimuthal angle of the π^+ in the ρ^0 centre of mass system. The angle ϕ is then that between the decay plane and the ρ^0 production plane (the γ^*–ρ plane). The angle Φ is that of the ρ^0 production plane with respect to the lepton scattering plane. SCHC hypothesises that the helicity of the virtual photon is retained by the ρ, in which case the angular distribution reduces to $W(\cos\theta, \psi)$ [26,28], where $\psi = \phi - \Phi$ is the angle of the ρ decay plane with respect to the lepton scattering plane.

For unpolarised electroproduction most of the density matrix elements were experimentally determined from the analysis of the moments of the distribution $W(\cos\theta, \phi, \Phi)$ [28]. In the present experiment, due to the limited statistics and complicated dependence of the acceptance on the angular variables, it was not feasible to perform a full multidimensional analysis of the angular distributions. We therefore limited the analysis to the single variable distributions in $\cos\theta$, ϕ and ψ.

3.5.1. The $\cos\theta$ distribution

After integrating $W(\cos\theta, \phi, \Phi)$ over ϕ and Φ the distribution is

$$W(\cos\theta) = \frac{3}{4}\left\{1 - r_{00}^{04} + (3r_{00}^{04} - 1)\cos^2\theta\right\} \tag{19}$$

and depends only on the density matrix element r_{00}^{04}, which can be identified as the probability that the ρ^0 was longitudinally polarised (i.e. helicity 0).

In Fig. 11 the $\cos\theta$ distributions, corrected for acceptance and normalised to unity, are shown. For all data sets a clear $\cos^2\theta$ dependence is observed indicating a substantial fraction of longitudinally polarised ρ^0 mesons. The curves represent fits of the function $W(\cos\theta)$ to the data.

The fitted values of r_{00}^{04} from this analysis are corrected for the contribution from the non-exclusive background. In the near inelastic region ($0.08 < I < 0.2$) the $\cos\theta$
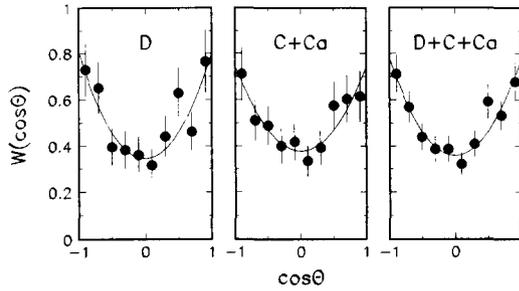
New Muon Collaboration/Nuclear Physics B 429 (1994) 503–529

Fig. 11. The $\cos\theta$ distributions for pions from the ρ^0 decay. The distributions are normalised to unity. The curves represent fits to the distributions (see text).
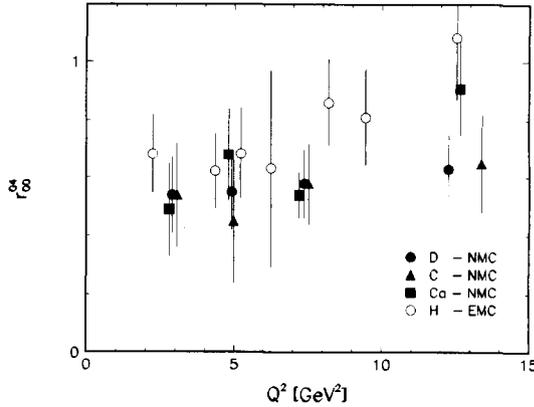

Fig. 12. The fraction of ρ^0 mesons with helicity 0 (r_{00}^{04}) as a function of Q^2. The data are from the present experiment for D, C and Ca (full symbols) and from the EMC [7] for the proton (open symbols).

distributions for ρ^0 decay are flat. We assume the same distribution for the background under the exclusive peak. The results for r_{00}^{04} are shown in Fig. 12 as a function of Q^2 for all the nuclei. No significant A dependence is observed. The average r_{00}^{04} for all Q^2 and all nuclei is 0.58 ± 0.04.

Also shown in Fig. 12 are the EMC data for the proton [7], which are in fair agreement with the present results. A direct comparison is however difficult as r_{00}^{04} may depend on the polarisation ϵ, for instance if s-channel helicity is conserved.

The coherent process on nuclei can be regarded as a "filter" for spin amplitudes, as in this case the spin-flip amplitudes are suppressed to a large extent. Then, if for exclusive ρ^0 production longitudinal virtual photons do not contribute, as suggested by Ref. [7], the values of r_{00}^{04} might be smaller for coherent than for incoherent events. To investigate this possibility samples of coherent and incoherent events were selected. The sample enriched in coherent events was obtained by applying an additional selection $p_t^2 < 0.05\ \text{GeV}^2$. The residual incoherent admixture in the coherent sample is about 10%. Likewise the incoherent sample was obtained by applying a selection $p_t^2 > 0.2\ \text{GeV}^2$
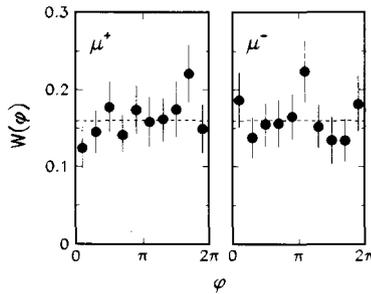
Fig. 13. The azimuthal angle ϕ distributions for pions from ρ^0 decay. The distributions are normalised to unity and are given separately for the data obtained with positive and negative incident muons. The dashed lines correspond to the uniform distributions expected if s-channel helicity conservation holds.

and replacing the standard inelasticity cut (3) by the restrictive inelasticity cut (5). The p_t^2 cut removes practically all coherent events and the inelasticity cut substantially reduces the non-exclusive background (cf. Sect. 3.3).

The values of r_{00}^{04} for the coherent and incoherent samples for all nuclei combined are 0.63 ± 0.07 and 0.64 ± 0.13 respectively. There is no indication of a difference for the two samples, which is consistent with the SCHC hypothesis for incoherent production.

3.5.2. The ϕ distribution

After integrating $W(\cos\theta, \phi, \Phi)$ over θ and Φ the distribution is

$$W(\phi) = \frac{1}{2\pi} \left\{ 1 - 2r_{1-1}^{04} \cos 2\phi + P\sqrt{1-\epsilon^2}\, 2\,\mathrm{Im}\, r_{1-1}^{3} \sin 2\phi \right\}, \tag{20}$$

where r_{1-1}^{04} and r_{1-1}^{3} are the ρ^0 density matrix elements, ϵ is the virtual photon polarisation and P polarisation of the muon beam. About equal amounts of data were taken with μ^+ and μ^- beams. These have opposite polarisations $P = \mp 0.82$ [29] so that two separate measurements of $W(\phi)$ were obtained.

The angle ϕ is subject to large kinematic smearing for events with small transverse momentum and so the ϕ distributions were analysed after removing events with $p_t^2 < 0.05$ GeV^2. For the remaining events the smearing is ≈ 150 mrad.

The ϕ distributions corrected for acceptance and combined for all nuclei are shown in Fig. 13 for both beam settings; they are normalised to unity. The dashed lines show the uniform distribution expected if s-channel helicity is conserved; in this case both r_{1-1}^{04} and r_{1-1}^{3} are predicted to be zero.

Simultaneous fits of Eq. (20) to both distributions yielded $r_{1-1}^{04} = -0.03 \pm 0.04$ and $\mathrm{Im}\, r_{1-1}^{3} = 0.02 \pm 0.07$, consistent with SCHC predictions.

3.5.3. The ψ distribution

As we mentioned, $W(\cos\theta, \phi, \Phi)$ takes a simpler form $W(\cos\theta, \psi = \phi - \Phi)$, if s-channel helicity is conserved. In this case, after integrating over $\cos\theta$, the distribution becomes
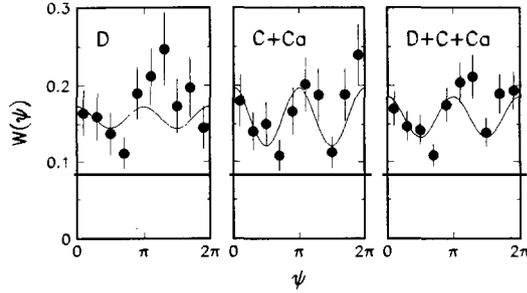
Fig. 14. The azimuthal angle ψ distributions for the pions from the ρ^0 decay. The distributions are normalised to unity. The curves represent the fitted decay angular distributions obtained assuming SCHC.

$$W(\psi) = \frac{1}{2\pi} \left\{ 1 + 2\epsilon r^1_{1-1} \cos 2\psi \right\}. \tag{21}$$

If, in addition to SCHC, there is natural parity exchange in the t channel, observed to be a good approximation at small Q^2 [3], r^1_{1-1} is related [26,28] to r^{04}_{00} by

$$r^1_{1-1} = \frac{1}{2}(1 - r^{04}_{00}). \tag{22}$$

The kinematic smearing of the angle ψ was acceptably small for all p^2_t, about 80 mrad.

The ψ distributions corrected for acceptance and normalised to unity are shown in Fig. 14. The curves show the results of the fits of $W(\psi)$ to the data with r^1_{1-1} as a free parameter. The quality of the fits is acceptable. The largest χ^2/NDF is 17/9, but if one assumes a uniform distribution, this becomes $\chi^2/NDF = 24/10$ which is significantly poorer. No significant A or Q^2 dependence was observed for r^1_{1-1} whose value was 0.16 ± 0.06 for the combined data. This value includes corrections for the non-exclusive background, which was assumed to have a uniform $W(\psi)$ distribution as suggested by the data in the near inelastic region. If we use Eq. (22) with the r^{04}_{00} measured in the present experiment, we obtain $r^1_{1-1} = 0.21 \pm 0.02$ in agreement with the fitted value.

3.5.4. Determination of R

The results on the ϕ and ψ distributions, as well as the similarity of r^{04}_{00} for coherent and incoherent events support the hypothesis of SCHC.

Assuming SCHC and using the measured r^{04}_{00} one can estimate the ratio R ($= \sigma_L/\sigma_T$ for exclusive virtual photoproduction) with the expression [28]

$$R = \frac{1}{\epsilon} \frac{r^{04}_{00}}{1 - r^{04}_{00}}. \tag{23}$$

From our combined data we obtain $R = 2.0 \pm 0.3$ at $\langle Q^2 \rangle = 6$ GeV^2.

This result may be compared to that of Ref. [7], $R = -0.38 \pm 0.13^{+0.9}_{-0.4}$ evaluated at $Q^2 = 2$ GeV^2 using, however, a different method. The two results are consistent with the increase of R with Q^2 predicted by many models [10–16].
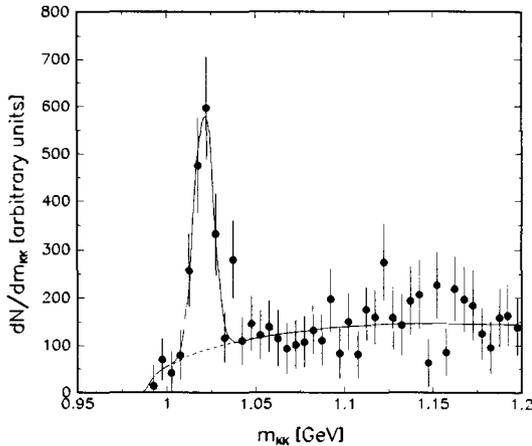
Fig. 15. Acceptance corrected distribution of the two-kaon invariant mass. The data from deuterium, carbon and calcium targets were combined. The full line represents the result of a fit assuming a superposition of a gaussian and a non-resonant contribution. The broken line shows the non resonant contribution parametrised as $a_0(m_{KK} - 2m_K)^{a_1}e^{-a_2 m_{KK}}$, where a_0, a_1, a_2 are fitted parameters and m_K is the charged kaon mass.

4. Exclusive ϕ production

4.1. The event sample

The procedure of selecting the sample of exclusive ϕ mesons was similar to that for exclusive ρ^0 mesons. Most of the cuts and selections were the same for both samples. Different cuts were applied on the invariant mass of the final state meson pair and the only other difference was in the method of suppressing electron background.

Cut (2) on $m^2_{e^+e^-}$, which was applied to the ρ^0 sample, could not be used here because of the overlap between ϕ events and photon conversions in the invariant mass spectra. Instead, to suppress electron background we used the measurements of energy deposited in the electromagnetic and hadronic parts of the calorimeter [19]. For each shower in the calorimeter, the ratio EMAGF (ElectroMAGnetic Fraction) of the energy deposited in the electromagnetic part to the total deposited energy, was calculated. The response of the calorimeter to electrons and hadrons was studied with both a sample of events with a single real photon (converting into e^+e^-), and with a sample of exclusive ρ^0 or ϕ events. For the showers initiated by electrons the EMAGF distribution peaks at values close to unity, whereas for hadrons the distribution favours smaller values. Thus, in order to suppress the electron background, the events were rejected if at least one track initiated a shower in the calorimeter with

$$\text{EMAGF} > 0.8. \tag{24}$$

This procedure leaves a residual electron background of about 2% of the data and results in a 3% uncertainty in the ϕ cross section.

The exclusive ϕ signal is shown in Figs. 15 and 16 for the combined data for the
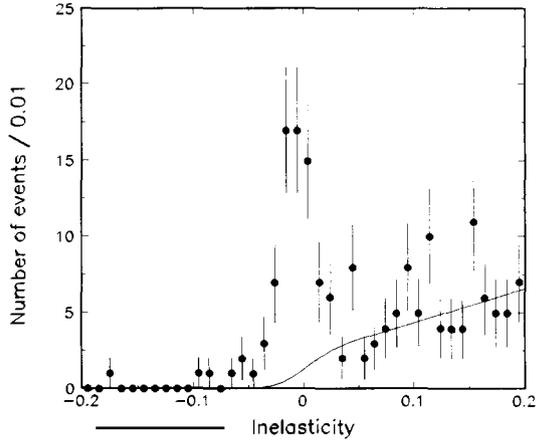
Fig. 16. Inelasticity distribution of ϕ mesons uncorrected for acceptance. The data from deuterium, carbon and calcium targets were combined. The solid line represents the parametrisation of the non-exclusive background described in the text.

three nuclei. In Fig. 15 the acceptance corrected distribution of the two kaon invariant mass m_{KK} is shown. The mass spectrum is not corrected for kinematic smearing. The data satisfy inelasticity cut (3) and the remaining selections of the ϕ sample except for the invariant mass cut. From the distribution we excluded those events which, for the hypothesis that the tracks are pions, gave the invariant mass $m_{\pi^+\pi^-}$ in the central region of the ρ mass ($0.695 < m_{\pi^+\pi^-} < 0.845$ GeV). The full line is the result of a fit to the data of a superposition of a gaussian and a non-resonant contribution. Satisfactory fits were obtained which yielded the ϕ mass $M_\phi = 1.0207 \pm 0.0009$ GeV and $\sigma = 0.0053 \pm 0.0008$ GeV. For the invariant mass range

$$1.005 < m_{KK} < 1.035 \, \text{GeV} \tag{25}$$

the fraction of non-resonant events is $(28 \pm 6)\%$. This background is reduced to $(19 \pm 6)\%$ if inelasticity cut (5) is used.

In Fig. 16 the inelasticity distribution uncorrected for acceptance is shown. The data satisfy the invariant mass cut (25) and the remaining selections of the exclusive ϕ sample except for the inelasticity cut. The signal of exclusive ϕ production is seen with non-exclusive events partially overlapping as for the ρ^0 case, cf. Fig. 3. The line is a parametrisation of the inelasticity distribution for non-exclusive events. It was obtained as for the ρ^0 sample (see Sect. 3.1). For the region defined by the inelasticity cut (3) the non-exclusive background contribution is $(22 \pm 11)\%$. With the restrictive inelasticity cut (5) it is reduced and equals $(3 \pm 4)\%$. These values are about the same as those for the ρ^0 sample.

We defined our ϕ sample using the kinematic cuts listed in Table 2, the vertex cuts, the cut on EMAGF, the invariant mass cut (25) and the inelasticity cut. Once again, for most of the analysis we used cut (3), except for the transverse momentum distributions, when cut (5) was used (cf. Sect. 3.3). The numbers of exclusive ϕ events obtained
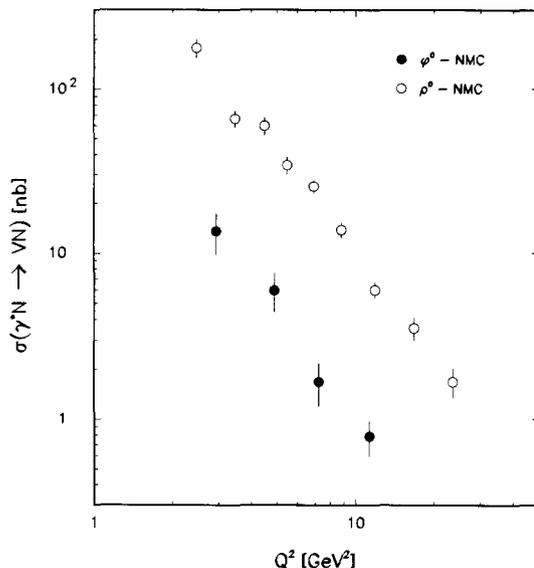
Fig. 17. The Q^2 dependence of exclusive vector meson virtual photoproduction cross sections. The data are for ϕ (full symbols) and for ρ^0 (open symbols) both from the present experiment. The cross sections are averaged over the three nuclei.

with cut (3) are given in Table 3.

The average values of Q^2 and ν for the ϕ sample are $\langle Q^2 \rangle = 6.4$ GeV^2 and $\langle \nu \rangle = 108$ GeV. They are close to the corresponding values for the ρ^0 sample.

4.2. Virtual photoproduction cross section as a function of Q^2

To extract the cross sections the same method as for the ρ^0 sample was used (Sect. 3.2). The cross section $\sigma_{\gamma^* N \to \phi N}(Q^2)$ was calculated according to a formula analogous to Eq. (9). The cross sections were corrected for detector acceptance, losses due to the secondary interactions of decay kaons in the target, non-exclusive and non-resonant backgrounds, efficiency of suppressing electron background and for the branching ratio of $\phi \to K^+ K^-$. In the corrections a possible correlation between the non-exclusive and non-resonant backgrounds was taken into account. Within the somewhat large errors we do not see any A dependence and only the combined cross sections for all nuclei are presented.

In Fig. 17 the Q^2 dependence of the cross section for exclusive ϕ virtual photoproduction is shown together with the cross section for exclusive ρ^0 production averaged over the three nuclei. The errors shown are statistical. Not shown are the systematic, mostly normalisation, errors which are about 20%. The cross section for ϕ production is about one order of magnitude smaller than that for ρ^0 production, but has a similar Q^2 dependence. The cross sections can be parametrised as $\propto (1/Q^2)^\beta$, with the parameter β equal to 2.27 ± 0.39 for ϕ and 2.02 ± 0.07 for ρ^0.
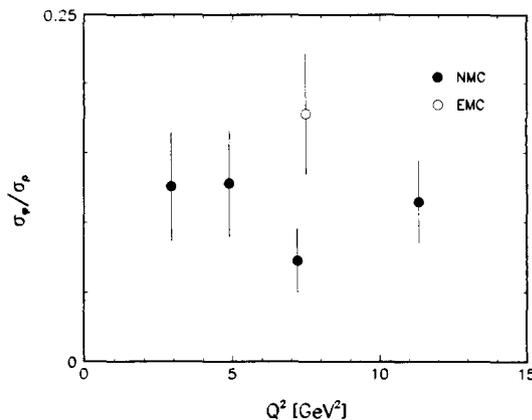
New Muon Collaboration/Nuclear Physics B 429 (1994) 503–529

Fig. 18. The ratio of the ϕ and ρ^0 meson production cross sections, σ_ϕ/σ_ρ as a function of Q^2. The data are from the present experiment for the deuterium, carbon and calcium combined (full symbols) and from the EMC for ammonia [8] (open symbols).

The ratio of the ϕ and ρ^0 meson production cross sections is shown as a function of Q^2 in Fig. 18 together with the result of a previous experiment [8]. The errors shown are statistical. The systematic error on this ratio is about 10%. One may expect the ratio σ_ϕ/σ_ρ to be related to the ratio of the squares of the charges of the valence quarks [3,8,16], which in this case is 2/9. The present results give a ratio which is about a factor two lower than this. It is interesting to note that the ratio of photoproduction cross sections ($Q^2 = 0$) is also about a factor two below the expectation of a quark-VMD model [3].

4.3. Transverse momentum distributions

The results presented in this section were obtained with the restrictive inelasticity cut (5), which reduces the non-exclusive background to about 3% at the expense of reducing the number of events by a factor of about two.

In Fig. 19 the acceptance corrected p_t^2 distributions of exclusive ϕ mesons are shown separately for the deuteron and for the combined data from the three nuclei. The distributions were obtained for $2 < Q^2 < 25$ GeV^2. The curves represent the fits to the exclusive ρ^0 data normalised to the ϕ data in the range $0.2 < p_t^2 < 1.0$ GeV^2. The comparison illustrates that incoherent ϕ production has less steep p_t^2 distributions than incoherent ρ^0 production. The p_t^2-slopes for the ϕ data were found by fitting a single-exponential dependence in the range $p_t^2 > 0.2$ GeV^2. The fitted values of the slopes are 3.4 ± 1.0 GeV^{-2} for the deuteron and 3.7 ± 0.9 GeV^{-2} for the combined data for the three nuclei. These values are smaller than the corresponding ones for ρ^0 production: 7.1 ± 0.9 GeV^{-2} for the deuteron and 6.3 ± 0.6 GeV^{-2} for the combined data (Table 6).
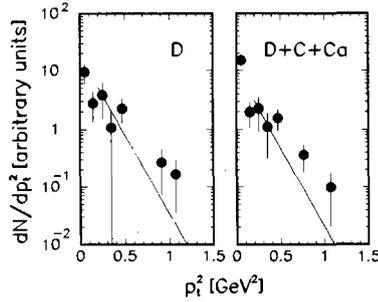
Fig. 19. The p_t^2 distributions for exclusive ϕ production for deuteron and the three nuclei combined. The distributions were obtained with a restrictive inelasticity cut (5) to reduce the effect of the non-exclusive background. The normalisation of each distribution is arbitrary. The line in each figure shows the p_t^2 slope for incoherent exclusive ρ^0 production from a fit to our combined data (see Sect. 3.3).
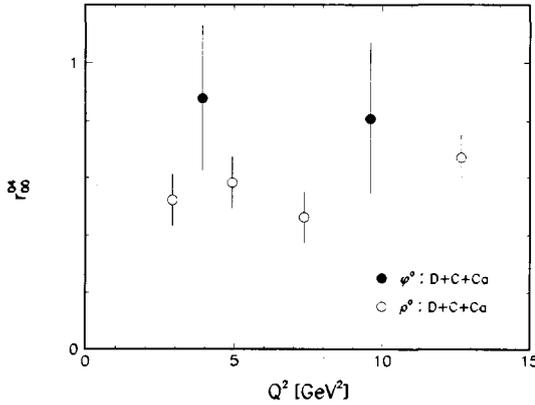
Fig. 20. The Q^2 dependence of the density matrix element r_{00}^{04} for ϕ (full symbols) and for ρ^0 (open symbols). The data were combined for deuterium, carbon and calcium.

4.4. Decay angular distributions

We only discuss the $\cos\theta$ distributions of the kaons from the decay $\phi \to K^+ K^-$. They display predominantly a $\cos^2\theta$ behaviour. Fitting Eq. (19) to the distributions for the combined data from all three nuclei yields the values of the matrix element r_{00}^{04} shown in Fig. 20. The ϕ data were corrected for the non-exclusive background as described for the ρ^0 case in Sect. 3.4. For comparison the values for the combined ρ^0 data are also shown in the figure. Over the whole Q^2 range the average r_{00}^{04} for the ϕ data is 0.84 ± 0.18 (for ρ^0 it is 0.58 ± 0.04). Though the errors on r_{00}^{04} for ϕ are large, there is an indication of a dominant contribution of longitudinally polarised ϕ.

5. Conclusions

We have studied exclusive ρ^0 muoproduction ($\mu N \to \mu \rho^0 N$) and exclusive ϕ muo-production ($\mu N \to \mu \phi N$) at large Q^2 (2–25 GeV^2) and in the ν interval 40–180 GeV. The data were taken with deuterium, carbon and calcium targets. The data from different nuclei have similar cross sections and distributions as a function of most of the kinematical variables except p_t^2.

The measured total cross sections for the process $\gamma^* N \to \rho^0 N$ as a function of Q^2 can be parameterised by a function $\propto 1/(Q^2)^\beta$, with β close to 2. We do not observe any significant ν dependence. The total cross section per nucleon can be parametrised as a function of A by $\sigma(A) = \sigma_0 A^\delta$, with $\delta = 0.035 \pm 0.032$.

The p_t^2 distributions of exclusive ρ^0 production exhibit a significant contribution from coherent events in addition to incoherent ones. For the range $0.2 < p_t^2 < 1.0$ GeV^2, we found that the p_t^2-slopes for incoherent distributions are about 6 GeV^{-2}. We observe no significant Q^2 dependence either of these slopes or of the ratio of coherent to incoherent total yields. The slopes are close to those for ρ^0 photoproduction and electroproduction at small Q^2 measured in previous experiments. Nuclear transparencies for carbon and calcium are significantly below unity.

From the analysis of the decay angular distributions we found that the fraction of longitudinally polarised ρ^0 mesons (helicity 0) is large. The decay azimuthal angular distributions and the similarity of the fractions of longitudinally polarised ρ^0 for the coherent and incoherent events are in agreement with s-channel helicity conservation (SCHC). Assuming SCHC and using the measured polar angular distributions we have estimated R, the ratio of the cross section to produce a ρ^0 by longitudinal virtual photons to that for transverse ones. The value of R is found to be 2.0 ± 0.3 at $Q^2 = 6$ GeV^2.

Most of the results of present paper are in fair agreement with those from the experiments of Refs. [6-8]. However, significant differences to the results of Refs. [7,8] were found for the slopes of the incoherent p_t^2 distributions as already reported in Ref. [1] and also for the fractions of coherent events.

The large slopes of the p_t^2 distributions for the incoherent cross sections, the approximate SCHC and the weak ν dependence observed in this experiment are characteristics of diffractive processes.

Exclusive ϕ production was also studied, using the decay channel $\phi \to K^+ K^-$. The production cross section is about an order of magnitude smaller than for the ρ^0, but its Q^2 dependence is similar. The p_t^2 distributions are less steep than those for the ρ^0. A large fraction of ϕ mesons is polarised longitudinally.

References

[1] NMC, P. Amaudruz et al., Z. Phys. C54 (1992) 239.
[2] For a review see e.g.
    A. Martin and G.Matthiae, *in* Proton–antiproton collider physics, eds. G. Altarelli and L. Di Lella (World Scientific, Singapore, 1989) p. 45.
[3] T.H. Bauer et al., Rev. Mod. Phys. 50 (1978) 261.
[4] CHIO, W.D.Schambroom et al., Phys. Rev. D 26 (1982) 1.
[5] H1 Collaboration, S. Levonian, *in* QCD and high energy hadronic interactions, Proc. XXVIII th Rencontre de Moriond, Les Arcs, France, 1993, ed. J. Trân Thanh Vân (Editions Frontières, Gif-sur-Yvette, 1993) p.529;
    ZEUS Collaboration, M.Costa, presentation at the Deep Inelastic Scattering Workshop, Eilat, Israel, 1994.
[6] E665, G.Y. Fang, *in* Proc. of Particle and Nuclei XIII International Conference, Perugia, Italy, 1993, ed. A. Pascolini (World Scientific, Singapore, 1994) p.332; FERMILAB-Conf 93/305 (1993); private communication.
[7] EMC, J.J. Aubert et al., Phys. Lett. B 161 (1985) 203.
[8] EMC, J. Ashman et al., Z. Phys. C 39 (1988) 169.
[9] R.J. Glauber, *in* Proc. Third International Conference on high energy physics and nuclear structure, ed. S. Devons (Plenum Press, New York, 1969) p. 207.
[10] A. Donnachie and P.V. Landshoff, Phys. Lett. B 185 (1987) 403.
[11] A. Donnachie and P.V. Landshoff, Nucl. Phys. B 311 (1989) 509;
    P.V. Landshoff, Nucl. Phys. B (Proc.Suppl.) 18C (1990) 211.
[12] P.V. Landshoff, *in* Proceedings of Joint Lepton-Photon Symposium and Europhysics Conference on High Energy Physics, Geneva, 1991, eds. S. Hegarty, K. Potter and E. Quercigh, Vol. 2 (World Scientific, Singapore, 1992) p. 363.
[13] J.R. Cudell, Nucl. Phys. B 336 (1990) 1.
[14] M.G. Ryskin, Z. Phys. C 57 (1993) 89.
[15] B.Z. Kopeliovich et al., Phys. Lett. B 324 (1994) 469.
[16] S.J. Brodsky et al., SLAC-PUB-6412, CU-TP-617, UCD-93-36 (1994), submitted to Phys. Rev. D.
[17] NMC, P. Amaudruz et al., Z. Phys. C 51 (1991) 387.
[18] NMC, D. Allasia et al., Phys. Lett. B 249 (1990) 366 and references cited therein;
    NMC, P. Amaudruz et al., Nucl. Phys. B 371 (1992) 3.
[19] EMC, O.C. Allkofer et al., Nucl. Instrum. Methods 179 (1981) 445.
[20] J.D. Jackson, Nuovo Cimento 34 (1964) 1644.
[21] Particle Data Group, Phys. Lett. B 239 (1990) II.4.
[22] NMC, P. Amaudruz et al., Phys. Lett. B 295 (1992) 159; CERN-PPE/92-124(1992) Erratum to CERN-PPE/92-124 (October 26,1992); Erratum to CERN-PPE/92-124 (April 19,1993).
[23] B. Badełek et al., TSL/ISV-94-0092(1994), to be published in Z. Phys. C.
[24] NMC, P. Amaudruz et al., Phys. Lett. B 332 (1994) 195.
[25] EMC, J. Ashman et al., Z. Phys. C 52 (1991) 361;
    EMC, J.J. Aubert et al. Phys. Lett. B 95 (1980) 306.
[26] K. Schilling and G. Wolf, Nucl. Phys. B 61 (1973) 381.
[27] J. Ballam et al., Phys. Rev. D 5 (1972) 545.
[28] P. Joos et al., Nucl. Phys. B 113 (1976) 53.
[29] EMC, J. Ashman et al., Nucl. Phys. B 328 (1989) 1.